References

1 PURSLEY, M.B.: 'Performance evaluation for phase-coded spread-spectrum multiple-access communication - Part I: System analysis', *IEEE Trans.*, 1977, **COM-25**, pp. 795–799

2 MAZZINI, G., SETTI, G., and ROVATTI, R.: 'Chaotic complex spreading sequences for asynchronous DS-CDMA - Part I: System modeling and results', *IEEE Trans.*, 1997, **CASI-44**, pp. 937–947

3 ROVATTI, R., SETTI, G., and MAZZINI, G.: 'Chaotic complex spreading sequences for asynchronous DS-CDMA - Part I: Some theoretical performance bounds', *IEEE Trans.*, 1998, **CASI-45**, pp. 496–506

4 ROVATTI, R., SETTI, G., and MAZZINI, G.: 'Toward sequence optimization for chaos-based asynchronous DS-CDMA systems'. Proc. IEEE GLOBECOM'98, Sydney, Australia, 1998

5 GRADSHTEYN, I.S., and RYZHIK, I.M.: 'Table of integrals, series, and products' (Academic Publishers, Boston 1994), 5th edn.

Iterative algorithm for nonuniform inverse fast Fourier transform (NU-IFFT)

Qing Huo Liu and Xue Yuan Tang

A nonuniform inverse fast Fourier transform (NU-IFFT) for nonuniformly sampled data is realised by combining the conjugate-gradient fast Fourier transform (CG-FFT) method with the newly developed nonuniform fast Fourier transform (NUFFT) algorithms. An example application of the algorithm in computational electromagnetics is presented.

Introduction: The fast Fourier transform (FFT) [1] is one of the most important algorithms in computational science and engineering. However, regular FFT algorithms are not suitable in many practical applications when the data are not uniformly sampled. Three different algorithms have been developed for the nonuniform fast Fourier transform (NUFFT) [2 – 4] which, for nonuniform $t_k \in [-N/2, N/2]$ and $\omega_j \in [-\pi, \pi]$, can evaluate the following summations for $j = -N/2, ..., N/2 - 1$:

$$f_j = \sum_{k=-N/2}^{N/2-1} \alpha_k e^{it_k 2\pi j/N} \equiv \sum_{k=-N/2}^{N/2-1} \alpha_k A_{jk} \qquad (1)$$

$$g_j = \sum_{k=-N/2}^{N/2-1} \beta_k e^{ik\omega_j} \equiv \sum_{k=-N/2}^{N/2-1} \beta_k B_{jk} \qquad (2)$$

with $O(m N\log_2 N)$ arithmetic operations (m is the oversampling rate). For convenience, we refer to the NUFFT algorithms in [4] for eqns. 1 and 2 as the NUFFT-1 and NUFFT-2 algorithms, respectively, for the nonuniformly spaced temporal points and frequency points.

For regular, uniformly sampled data where both $\{t_k\}$ and $\{w_j\}$ are uniform, the inverse FFT (IFFT) can share the same algorithm as the FFT simply because $A^{-1} = A^\dagger/N$ and $B^{-1} = B^\dagger/N$ in these special cases (where superscript † denotes the complex conjugate and transpose of a matrix). Unfortunately, this is no longer true for matrices A and B for nonuniformly sampled data. Hence, the nonuniform inverse FFT (NU-IFFT) can no longer share the same algorithm as the NUFFT. Obviously, the direct inversion of eqn. 1 and eqn. 2 to obtain α_k and β_k is prohibitively expensive since it requires $O(N^3)$ arithmetic operations. In this work, we use the conjugate-gradient and regular FFT (CG-FFT) method together with the NUFFT algorithms to develop an accurate NU-IFFT algorithm.

Formulation: We first rewrite eqn. 1 using matrix notation $f = A\alpha$. From elementary matrix identities we observe that $A^{-1} = A^\dagger(AA^\dagger)^{-1}$. Therefore the inverse DFT solution of eqn. 1 is

$$\begin{aligned} \alpha &= A^\dagger h \\ h &= (AA^\dagger)^{-1} f \end{aligned} \qquad (3)$$

The advantage of rewriting the solution in the form of eqn. 3 is clear because matrix $AA^\dagger$ is a Toeplitz matrix [2], i.e. $(AA^\dagger)_{jl} = a_{j-l}$, where

$$a_j = \sum_{k=-N/2}^{N/2-1} e^{it_k 2\pi j/N} \qquad j = -N+1, ..., N-1 \qquad (4)$$

Observe that there are only N independent elements in array a since $a_{-j} = (a_j)^*$. Furthermore, these N elements in eqn. 4 can be obtained by the NUFFT-1 algorithm

$$a_{j+N/2} = \sum_{k=-N/2}^{N/2-1} d_k e^{it_k 2\pi j/N} \qquad j = -N/2, ..., N/2 - 1 \qquad (5)$$

where $d_k = \exp(i\pi t_k)$, with $O(m N\log_2 N)$ arithmetic operations.

Since $AA^\dagger$ is a Toeplitz matrix, the vector h in eqn. 3 can be obtained efficiently using the conjugate-gradient FFT (CG-FFT) method (see [5], for example). In the CG-FFT method, the solution of h in eqn. 3 is obtained iteratively. Each iteration involves operations such as $y = (AA^\dagger)x$ which can be written as a discrete convolution:

$$y_j = \sum_l a_{j-l} \cdot x_l = \{FFT^{-1}[FFT(a)FFT(x_p)]\}_j \qquad (6)$$

and has been calculated by the regular FFT algorithm through the convolution theorem. Note that in eqn. 6, the size of the FFTs is $2N$, and x_p is the array x padded with N zeros. After h is solved by the above CG-FFT method, we can obtain α from eqn. 3 by

$$\alpha_j = \sum_{k=-N/2}^{N/2-1} A_{kj}^* h_k = \left[\sum_{k=-N/2}^{N/2-1} h_k^* e^{ik\frac{2\pi t_j}{N}} \right]^* \qquad (7)$$

which can be achieved by the NUFFT-2 algorithm.

In summary, the procedures for the NU-IFFT algorithm for eqn. 1 are:

(i) *Preprocessing*: to use the NUFFT-1 for array $\{a_j\}$ through eqn. 5, and to use the FFT algorithm to find [FFT(a)]

(ii) *Inversion*: to use the CG-FFT method to find a solution for h in eqn. 3

(iii) *Transposition*: to apply the NUFFT-2 to the transposed problem in eqn. 7.

In these procedures, since NUFFT-1 and NUFFT-2 require $O(m N\log_2 N)$ arithmetic operations, the most expensive step is the CG-FFT solution. It requires $O(KN\log_2 N)$ arithmetic operations, where the number of iterations K in the CG method is proportional to the condition number of $AA^\dagger$. In most applications, K is rather small as the points $\{t_k\}$ are fairly uniformly spaced. A similar algorithm has been developed for the NU-IFFT of eqn. 2.

Numerical results: We first compare the algorithm in [2] and our algorithm with cosine accuracy factors, and $N = 64$, $m = 2$, and $q = 8$. The input frequency-domain data f_j and the locations of the temporal sample points are both obtained by a pseudorandom number generator with a large variation. The absolute errors in our NU-IFFT algorithm are almost an order of magnitude smaller than those in the algorithm in [2], as shown in Fig. 1. Quantitatively, the L_2 and L_∞ errors are $E_2 = 1.64 \times 10^{-5}$, $E_\infty = 7.17 \times 10^{-7}$ in our NU-IFFT algorithm, and $E_2 = 1.26 \times 10^{-4}$, $E_\infty = 4.81 \times 10^{-6}$ using the algorithm in [2].

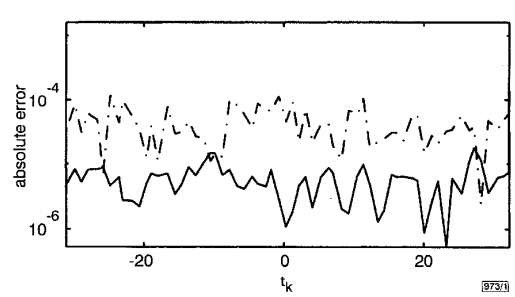

Fig. 1 *Comparison of absolute error in NU-IFFT result with that in [2] for random input array*

Direct result is $\alpha_k = (1 + i)[r(k) - 0.5]$ at $t_k = k + r(k)/2$, where $r(k)$ is random number with uniform distribution in [0, 1]
– · – · – D-R
——— NU-IFFT

As an example of applications, the NU-IFFT algorithm is used to reconstruct the spatial electric field distribution near a high-contrast dielectric slab located between $x = -1.5$ and $x = 1.5$m.

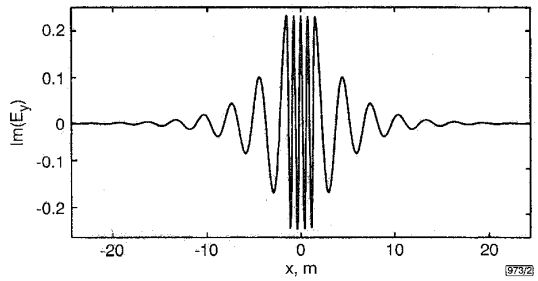

Fig. 2 *Reconstruction of imaginary part of spatial field distribution and exact solution near a dielectric slab over $-1.5 \le x \le 1.5m$*

The real part has a similar accuracy. The sample points for $-2.4268 \le x \le 2.3810$m are twice as dense as the rest of the domain
——— exact
– – – – NU-IFFT

The dielectric constant of the slab is $\epsilon_r = 16$, and the background medium is conductive with $\epsilon_r = 1$ and $\sigma = 0.0015$S/m. A planar electric current source J_y is located at $x = -1.548$m and excites waves at 100 MHz. By re-sampling the analytically calculated spatial spectrum of the electric field $\tilde{E}_y(k_x)$, we use the NU-IFFT algorithm ($N = 562$, $m = 2$, $q = 8$) to reconstruct the spatial field distribution over a set of nonuniform spatial points $\{x_k\}$. For simplicity, the distribution of these $\{x_k\}$ points is chosen such that the sampling rate near and inside the slab (where high-frequency oscillations exist) is twice that away from the slab. As shown in Fig. 2, the NU-IFFT reconstructed field distribution has an excellent agreement with the exact solution. The maximum relative error in the reconstruction is 0.66%, and the number of CG iterations is $K = 28$.

Conclusions: Using the CG-FFT method and the NUFFT algorithms based on the regular Fourier matrices, we develop an inverse fast Fourier transform (NU-IFFT) algorithm for nonuniformly spaced data. With a comparable complexity of $O(KN\log_2 N)$ (where K is the number of CG iterations), our NU-IFFT algorithm is more accurate than the previously reported results. An example in the field reconstruction near a high-contrast dielectric slab is shown to demonstrate the application of the NU-IFFT algorithm.

Acknowledgments: This work was supported by U.S. EPA through a PECASE grant CR-825-225-010, and by the NSF through a CAREER grant ECS-9702195.

© IEE 1998
4 August 1998
Electronics Letters Online No: 19981372

Qing Huo Liu and Xue Yuan Tang (*Klipsch School of Electrical and Computer Engineering, New Mexico State University, Las Cruces, NM 88003, USA*)

References

1 COOLEY, J.W., and TUKEY, J.W.: 'Algorithm for the machine computation of complex Fourier series', *Math. Comp.*, 1965, **19**, pp. 297–301

2 DUTT, A., and ROKHLIN, V.: 'Fast Fourier transform for nonequispaced data', *SIAM J. Sci. Comput.*, 1993, **14**, pp. 1368–1393

3 BEYLKIN, G.: 'On fast Fourier transform of functions with singularities', *Appl. Comput. Harmonic Analysis*, 1995, **2**, pp. 363–381

4 LIU, Q.H., and NGUYEN, N.: 'An accurate algorithm for nonuniform fast Fourier transforms (NUFFT's)', *IEEE Microw. Guid. Wave Lett.*, 1998, **8**, pp. 18–20

5 CÁTEDRA, M.F., TORRES, R.P., BASTERRECHEA, J., and GAGO, E.: 'The CG-FFT method: Application of signal processing techniques to electromagnetics' (Artech House, Boston, 1995)

Long term fading in direct sequence spread spectrum in microcellular environments

M.P. Fitton, M.A. Beach and A.R. Nix

The shadowing (or long term) statistics of a wireless system have a large impact on overall performance. The authors show experimentally that the inherent path diversity of a direct sequence spread spectrum system will reduce the effect of long-term envelope variation due to shadowing. This will result in a network with more homogeneous quality-of-service, reduce handovers, and improve capacity.

Introduction: Direct sequence code division multiple access (DS-CDMA) techniques are widely employed for a variety of wireless communications [1]. The advantages include robust multiple access and the provision of path diversity, for example through the use of a RAKE receiver [2]. The propagation aspects of employing a large transmission bandwidth are manifold, and include increased path diversity [2] and the mitigation of power control errors [3].

It has been demonstrated that, as the spreading bandwidth increases, the fast fading characteristic of each diversity path becomes more deterministic [2]. However, in this Letter it is illustrated that the long term (shadowing) characteristic will also become more deterministic when employing a large spreading bandwidth and path diversity. In this analysis, a real microcellular environment was rigorously characterised [4], including deeply shadowed and street-corner regions.

The importance of shadowing (or long-term fading) is far reaching and well understood [3]. The effects of buildings, hills, vegetation and other obstructions surrounding the transmitter and receiver can cause large envelope variations over distances of several metres. In a microcellular environment, it is likely that a number of paths arriving at the receiver will possess largely independent shadowing. This arises as propagation is largely confined to street-canyons [3], resulting in significant angular spread of multipath components, and low correlation, as shown later.

In a narrowband system, the composite long-term fading that is observed will result from a vector summation of all significant multipath components arriving at the receiver. In the case of DS-spread spectrum (DS-SS), the multipath components can be resolved to a certain extent through path diversity, with each time bin displaying largely independent shadowing. The composite long-term fading will result from a coherent addition of co-phased path diversity bins in the receiver. The summation of a large number of co-phased shadowing components will display less variation than the narrowband case, following the central limit theorem. The improvement in shadowing will depend on the channel profile, time resolution and path diversity order.

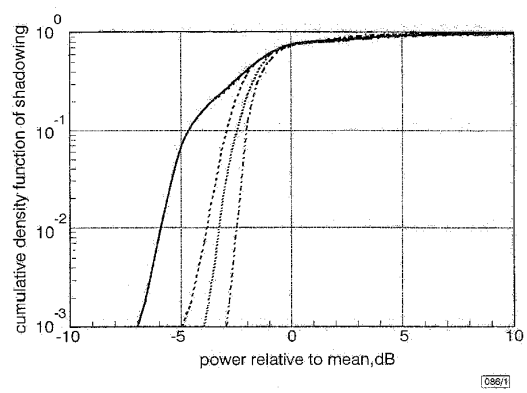

Fig. 1 *Shadowing statistics for various spreading bandwidths*

——— narrowband
– – – – 1.25 MHz
..... 4 MHz
– · – · 8 MHz

Propagation measurements: In a deeply shadowed region, the receiver has no line-of-sight path, and no large variations in surrounding obstructions occur. The narrowband shadowing standard deviation is 3.6dB, which agrees with previous research [5].